Journal of Power Sources 253 (2014) 263–268

Contents lists available at ScienceDirect

Journal of Power Sources

journal homepage: www.elsevier.com/locate/jpowsour

Polysulfide shuttle control: Towards a lithium-sulfur battery with superior capacity performance up to 1000 cycles by matching the sulfur/electrolyte loading

Xin-Bing Cheng, Jia-Qi Huang*, Hong-Jie Peng, Jing-Qi Nie, Xin-Yan Liu, Qiang Zhang*, Fei Wei

Beijing Key Laboratory of Green Chemical Reaction Engineering and Technology, Department of Chemical Engineering, Tsinghua University, Beijing 100084, China

HIGHLIGHTS

- The polysulfide shuttle was tuned by the loading of sulfur and electrolyte.
- A high initial discharge capacity of 1053 mAh g^{-1} at a high rate of 1 C.
- An ultralow decay rate of 0.049%/per cycle during 1000 cycles.
- The polysulfide shuttle was suppressed to a shuttle factor of 0.02.

GRAPHICAL ABSTRACT

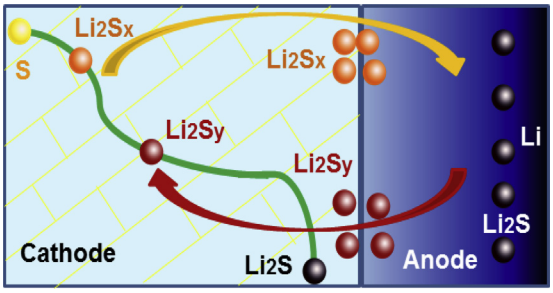

ARTICLE INFO

Article history:
Received 9 October 2013
Received in revised form
21 November 2013
Accepted 7 December 2013
Available online 16 December 2013

Keywords:
Lithium sulfur battery
Shuttle
Polysulfide
Cycle life
Electrolyte
Carbon nanotube

ABSTRACT

Lithium-sulfur battery is one of the most promising alternative power sources, but the polysulfide shuttle between the anode and cathode induces low Coulombic efficiency, low utilization of the sulfur cathode, and severe degradation of cycle life. Herein, the polysulfide shuttle was tuned by the loading of sulfur and electrolyte in a Li-S cell. A lithium-sulfur cell with a high initial discharge capacity of 1053 mAh g^{-1} at a high rate of 1 C and an ultralow decay rate of 0.049%/per cycle during 1000 cycles was obtained by using carbon nanotube@sulfur cathode and suppressing polysulfide shuttle to a shuttle factor of 0.02 by matching the sulfur/electrolyte loading. The use of matching the sulfur/electrolyte loading is a facile way to tune the shuttle of polysulfide, which provides not only new insights to the energy chemistry of Li/S batteries, but also important principle to assemble a Li/S cell with recommend loading for their commercialization application in portable mobile devices and electric vehicles.

© 2013 Elsevier B.V. All rights reserved.

1. Introduction

The energy from the fossil fuels brings the flourish of mankind. However, the vast consumption of fossil-fuel causes the rapid decrease of its holding and increasing pollution of environment [1,2]. High-capacity energy storage systems are highly desirable to meet the requirement of electric vehicles and utilization of renewable energies like solar or wind energies. The broad applications of portable batteries in cell phones or laptops as well as large-packaged batteries in electric vehicles requires energy storage systems with high energy density, good safety, and low cost [3]. Li-ion batteries, which are approaching their theoretical specific

* Corresponding authors. Tel.: +86 10 6278 9041; fax: +86 10 6277 2051.
E-mail addresses: jqhuang@tsinghua.edu.cn (J.-Q. Huang), zhang-qiang@mails.tsinghua.edu.cn (Q. Zhang).

0378-7753/$ – see front matter © 2013 Elsevier B.V. All rights reserved.
http://dx.doi.org/10.1016/j.jpowsour.2013.12.031

capacity at around 100–200 mAh g^{-1} based on the cathode's active material for traditional intercalation materials, cannot meet these requirements. With a theoretical capacity of 1675 mAh g^{-1}, elemental sulfur has been considered as one of the most promising alternative cathode materials [2,4,5]. The use of sulfur cathode has low cost, a low toxicity, and abundant resource [1,6,7]. Li–S batteries have a gravimetric energy density being the same or 2–3 times as high as Li-ion batteries.

However, the practical application of Li/S batteries is greatly hampered by some persistent problems including (1) sulfur and discharge products (Li_2S_2 and/or Li_2S) has a low electrical conductivity, affecting the reaction rate of the battery; (2) the Li_2S and other insoluble compounds are generated and cover the active compounds during cycling, which inhibits access of lithium ions and degrades the conductive network, and (3) the high-order soluble polysulfides can penetrate through the separator to the lithium negative electrode, where they are reduced to insoluble Li_2S or Li_2S_2, and the following polysulfides react with these fully reduced sulfides to form lower-order polysulfides, which become concentrated at the anode side and diffuse back to the positive electrode and are then re-oxidized into high-order polysulfides [7]. Such shuttle between the anode and cathode induces deposition of solid Li_2S_2 and Li_2S on the anode and loss of the active material, which leads to low Coulombic efficiency, low utilization of the sulfur cathode, and severe degradation of cycle life.

To overcome these problems, many efforts have been explored to enhance the electrical conductivity of the cathode and suppress the loss of soluble polysulfide intermediates during cycling. The use of conductive nanocarbon (*e.g.* mesoporous carbon [8–11], carbon nanotubes (CNTs) [12–16], graphene [1,17–19], CNT/graphene hybrids [20], carbon hollow spheres [21], etc.) and polymers (Polyaniline [22,23], polyacrylonitrile [24], etc.) gives rise to advanced composite cathode with excellent conductivity, robust electron/ion pathway, as well as superior reversible charge–discharge capacity and cycling performance [5]. Up to now, how to retard the shuttle of polysulfides is still a key issue to obtain Li–S cells with superior Li storage performance. On one hand, the incorporation of polymer chains (such as polyethylene glycol [8,18,25], polyvinylpyrrolidone [16]) or porous polysulfide reservoirs [26] affords the surface of nanocarbon/sulfur cathode to become highly hydrophilic and a chemical gradient is constructed that the polysulfides would preferentially be trapped by oxygen-containing groups on the cathode surface instead of dissolving in the bulk electrolyte. Therefore, the concentration of polysulfide in the electrolyte inclines to be lower, and the redox shuttle is partially inhibited. On the other hand, an electrolyte with a highly concentrated lithium salt [27,28] or solvent-in-salt electrolyte [29] with ultrahigh salt concentration and high lithium-ion transference number were employed, in which salt holds a dominant position in the lithium-ion transport system; consequently, the polysulfide dissolution from the cathode can be easily controlled by the common ion effect, and a high discharge capacity with good cyclic capacity retention is available. The introduction of tetrabutylammonium triflate or *N*-methyl-*N*-butylpyrrolidinium bis(trifluoromethanesulfonyl)imide is expected to stabilize the polysulfide anions through a chemical interaction between the soft acid and soft base [30], and the $LiNO_3$ participates in the formation of a stable passivation film to effectively suppress the redox shuttle of the dissolved lithium polysulfides on Li anode [31]. However, the dissolution of polysulfide in a Li/S cell is highly dependent on the sulfur/electrolyte loading [32]. How to well fit the loading of sulfur and electrolyte to retard the shuttle of polysulfide is not well understood yet.

In this contribution, the fitting between CNT@S cathode and electrolyte was explored. The reason we select CNT@S cathode with excellent Li ion storage performance is that the CNTs with quite high electrical conductivity, tunable pore size distribution, and robust scaffolds had been mass-produced by fluidized bed chemical vapor deposition at a very low cost of less than 100 $ kg^{-1} [33,34], which is quite potential for the commercial industrial applications of Li/S cells. Herein, the mixed solution of the 1,3-dioxolane (DOL) and 1,2-dimethoxyethane (DME) ($v/v = 1/1$) with 1 mol L^{-1} lithium bis(trifluoromethanesulfonyl)imide (LiTFSI) was selected as the electrolyte. This is most popular electrolyte that is accepted for Li/S cells by many research groups due to its solvability of polar polysulfides and appropriate ion mobility, although its Coulombic efficiency is less than 90% in most case.

2. Experimental

The CNT@S cathode was prepared by a facile co-heating procedure similar to our previous reports [14,20]. The CNTs was mass-produced on a Fe based catalyst in a fluidized bed reactor, and routine purification was carried out to remove the residual catalyst [35]. The sulfur was mixed with the CNTs by ball milling for 3 h, and the as-obtained mixtures were set in a sealed bottle. The bottle was heated to 155 °C and maintained for 1.0 h, which allows sulfur to immerse into the CNT scaffold and form CNT@S cathode.

A JSM 7401F scanning electron microscopy (SEM, JEOL Ltd., Tokyo, Japan) at 1.0 kV and a transmission electron microscopy (TEM, JEOL Ltd., Tokyo, Japan) at 120.0 kV were employed to detect the morphology of cathodes. The Raman spectra of the CNT and CNT@S cathode were recorded using Horiba Jobin Yvon LabRAM HR800 Raman spectrometer (He–Ne laser excitation at 633 nm). The sulfur content of CNT@S electrode was determined by thermogravimetry analysis (TGA) using TGA/DSC1 STAR^e system with N_2 atmosphere and a temperature ramp rate of 10 °C min^{-1}. The N_2 adsorption–desorption isotherms were collected by using an N_2 adsorption analyzer (Autosorb-iQ_2-MP-C system) at 77 K. The sample was degassed at a low temperature of 50 °C until a manifold pressure of 2 mm Hg was reached before N_2 sorption isotherm measurements to avoid the sulfur sublimation. The surface area was determined by the Brunauer–Emmett–Teller (BET) method, and the pore size distribution plot was available by the nonlocal density functional theory and Monte-Carlo method.

The composite CNT@S cathode was fabricated with PVDF binder in NMP with a mass ratio of CNT@S: PVDF = 85:15. A homogeneously mixed slurry was prepared by magnetic stirred for *ca.* 24.0 h. The as-obtained slurry was coated onto a 25 μm thick Al current collector by a doctor blade. The obtained electrode was dried in a vacuum drying oven at 60 °C for 12.0 h. After that, the foil was punched into 13 mm disks as the working cathodes. According to the SEM image, the thickness of the cathode electrode was 10–15 μm excluding the thickness of Al current collector. The electrodes were assembled in a two-electrode cells configuration using standard 2025 coin-type cells. 1 mm thick Li metal foil was selected as a counter electrode. The mixed solution of DOL and DME ($v/v = 1/1$) with 1 mol L^{-1} Lithium bis(trifluoromethanesulfonyl)imide (LiTFSI) as the electrolyte, and the Celgard 2400 polypropylene membranes as the separator. The assembling of cells was conducted in an Ar-filled glove box with oxygen and water content below 1 ppm. The coin cells were monitored in galvanostatic mode within a voltage range of 1.6–3.0 V using Neware multichannel battery cycler. To increase the discharge capacity of CNT/S cathode and Coulombic efficiency, an electrolyte with 0.1 M Li_2S_5 (with [S] = 0.5 M) and 0.5 M lithium nitrate ($LiNO_3$) dissolved in the above mentioned DOL/DME with 1 mol L^{-1} LiTFSI electrolyte was employed. Unless otherwise noted, the capacities hereafter are normalized to the sulfur content in the cathode. The amount of Li_2S_5 in the electrolyte was also calculated as the sulfur source.

3. Results and discussion

The CNT@S composites employed herein illustrated coaxial nanocable morphology (Fig. S1a), while sulfur uniformly coated on the conductive CNT scaffold (Fig. S1b). The CNTs were served as robust conductive networks, and well-preserved interpenetrated architectures offered the interconnected channels for electrolyte wetting and fast ion diffusion. No vibration peak of sulfur was detected in the Raman spectrum of CNT@S composites, and only weak and broaden diffraction peak of orthorhombic sulfur phase was observed in the X-ray diffraction pattern (Fig. S1c, d), indicating the sulfur was uniformly distributed on the conductive network. From thermogravimetry (TG) profile, high sulfur loading with 53.6% was obtained (Fig. S1e).

The thickness of the electrode was controlled by the doctor blade method, and the electrolyte volume was tuned to obtain Li/S cells with different sulfur loading concentrations ([S]). The [S] was defined as the ratio of molar amount of sulfur in the CNT@S composite cathode to the volume of electrolyte encapsulated in an individual cell. An obvious dependence of discharge capacity *vs.* the sulfur loading was shown as Fig. 1a. The initial discharge capacities of CNT@S were 854, 1026, 1098, and 803 mAh g^{-1} at a [S] of 0.34, 0.51, 1.12, and 2.58 mol L^{-1}, respectively. As shown in the galvanostatic charge–discharge profiles of 2nd cycle (Fig. 1b), there are two discharge stages: the reduction of sulfur to polysulfide in the first stage ($S_8 + Li^+ + e^- \rightarrow Li_2S_x$ (about 2.4 V, $4 \leq x \leq 8$)), and the further reduction of polysulfide into lithium sulfide in the second stage ($Li_2S_x + Li^+ + e^- \rightarrow Li_2S_2$ and/or Li_2S (around 2.1 V, $x \leq 4$)). When employing a large amount of electrolyte and correspondingly low sulfur loading of 0.34 M, the Coulombic efficiency was ultralow of 35.0%, while the charge and discharge capacities were 2435 and 853 mAh g^{-1}, respectively. The dissolved polysulfides in

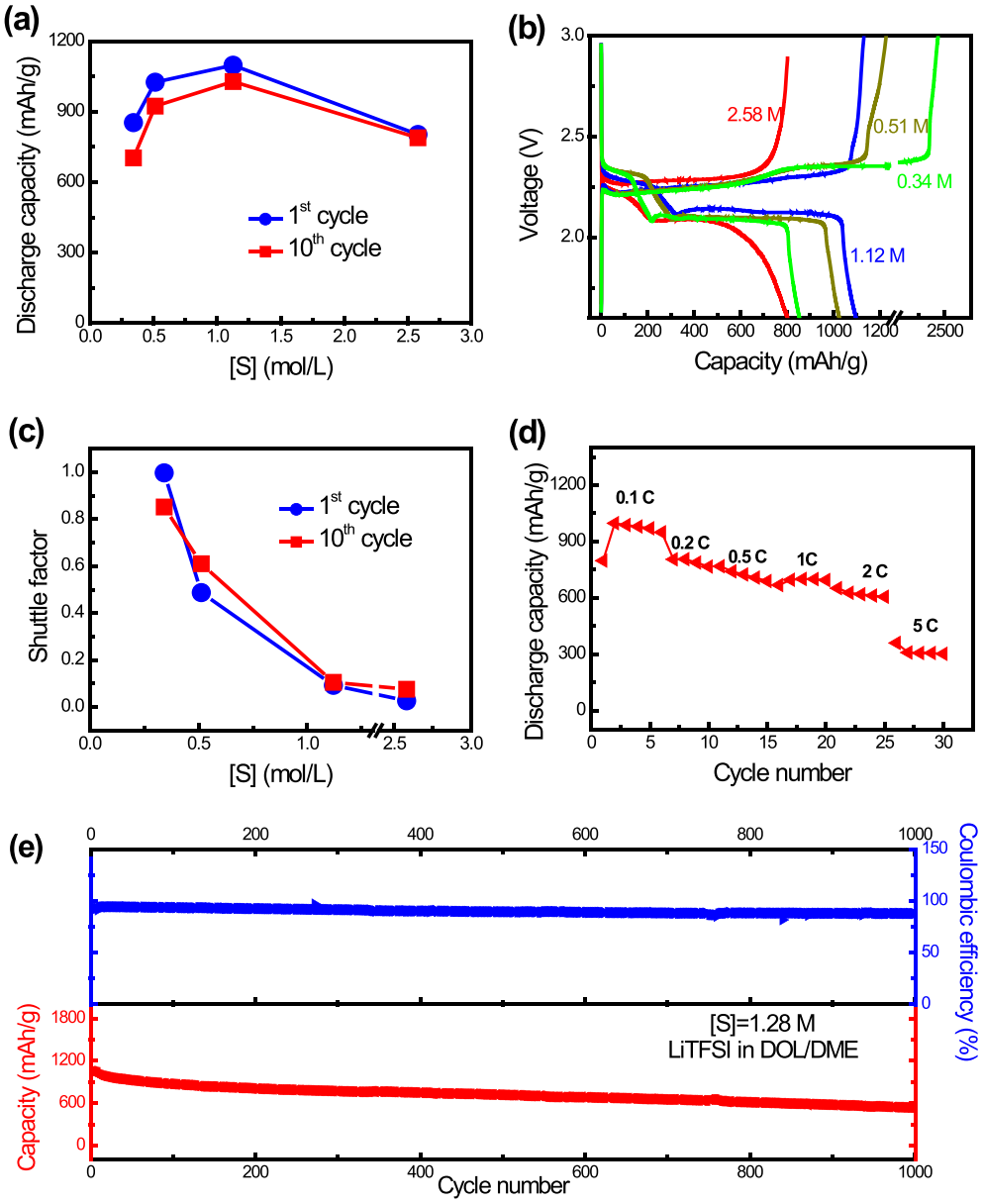

Fig. 1. (a) The relationship between the initial and 10th discharge capacity at a current rate of 0.1 C vs. the sulfur loading amount based on DOL/DME electrolyte in a Li/S cell. (b) The Galvanostatic charge-discharge profiles of the 2nd cycle of DOL/DME electrolyte at a current rate of 0.1 C. (c) The dependence of shuttle factor on the sulfur loading amount in a Li/S cell. (d) The rate performance of CNT@S cathode at the optimized [S]. (e) The cycling performance of CNT@S cathode with a sulfur loading of [S] = 1.28 M in the DOL/DME electrolyte at a current density of 1 C.

the electrolyte give rise to a redox shuttle phenomenon inside the cell due to their spontaneous reduction and oxidation and freely diffusion in the electrolyte between the anode and cathode. The reduction of the polysulfides may form an insoluble Li_2S_2 and/or Li_2S film on the metallic lithium, which can create a barrier to Li-ion diffusion, lower the utilization of active mass, and thus, degrade the overall cell performance [36]. In contrast, as decreasing the electrolyte amount to a relatively high sulfur loading of 1.12 mol L^{-1}, the precipitation and dissolution equilibrium ensured that the concentration of dissolved polysulfides was quasi-dynamically balance. Therefore, the amount of dissolved polysulfides would be reduced with less electrolyte employed. As a result, a high Coulombic efficiency of 97.3%, charge and discharge capacities of 1128 and 1098 mAh g^{-1} were available. The voltage platform of polysulfide reduction increased from 2.09 to 2.14 V, while the voltage platform of sulfide/disulfide oxidation almost remained the same. Such alleviated polarization of reversible polysulfide reduction/oxidation indicated that the high concentration of polysulfide during discharge/charge process facilitated the transfer of polysulfide to the electrode/electrolyte interface and the utilization of sulfur. The Coulombic efficiency was increased to 99.1% when the [S] was further increasing to 2.58 mol L^{-1} via decreasing the amount of electrolyte, also ascribing to the equilibrium theory; however, the full infiltration of the electrolyte to the CNT@S cathode became difficult, and such poor wetting induced an obviously decreased discharge capacity.

The diffusion behavior of high-order polysulfides at different sulfur loading concentrations were quite different. The shuttle effect was considered as the competition between the electrochemical reactions macroscopically performed as the charge/discharge current and the thermodynamically spontaneous diffusion of polysulfides from cathode to anode, and a shuttle factor proposed by Mikhaylik and Akridge [37] was defined to reflect the extent of shuttle effect as follows:

$$f = k_s \cdot Q_H / I \quad (1)$$

where k_s is the heterogeneous reaction constant related with polysulfide diffusion and reaction, Q_H is the theoretical charge/discharge capacities of the high plateau, and I is the charge/discharge current. Based on the assumptions reported in the previous literature [36], the Coulombic efficiency (C_{eff}) was a function of the shuttle effect:

$$C_{eff} = \frac{2 + (\ln(1+f))/f}{2 - (\ln(1-f))/f} \quad (2)$$

The shuttle factor can be calculated based on the Coulombic efficiency of cells at different sulfur loading concentrations while larger shuttle factor implied severer shuttle effect. When the [S] was 0.34 mol L^{-1}, a shuttle factor of 0.9965 was available, indicating that most of polysulfides shuttled between anode and cathode infinitely, resulting in a very low discharge capacity and conceivably fast capacity degradation. The shuttle factor monotone decreased with the rise of [S] in a cell (Fig. 1c). The shuttle of polysulfides was retarded when the [S] became higher. The 1st cycle shuttle factor of CNT@S cathode at a [S] of 0.34 mol L^{-1} is larger than the 10th cycle, which is attributed from the heavily dissolution of polysulfides and a large amount of Li_2S_2/Li_2S were irreversible deposited on the anode at the initial cycles. With the increasing of [S], the 10th cycle shuttle factors of CNT@S cathode are larger than the initial cycle. Decay rates of 1.76, 0.99, 0.63, 0.18% of initial capacity/per cycle were observed on the CNT@S cathode during the initial 10 cycles with [S] of 0.34, 0.51, 1.12, 2.58 mol L^{-1}, respectively.

Fig. 1d showed good rate performance with the optimized sulfur/electrolyte loading, which revealed a capacity of 998, 949, 768, 668, 652, 360 mAh g^{-1} at the current density of 0.1, 0.2, 0.5, 1, 2, and 5 C (1 C = 1675 mAh g^{-1}), respectively. A long cycling test was conducted at a current density of 1675 mA g^{-1} (1 C rate) (Fig. 1e). An initial discharge capacity of 1053 mAh g^{-1} was delivered and after 1000 cycles, a discharge capacity of 535 mAh g^{-1} was still preserved on CNT@S cathode with a sulfur loading of [S] = 1.28 M at a current density of 1 C. This is available in the DOL/DME electrolyte without addition of $LiNO_3$ or replacing the metallic lithium electrode and/or separator. The decay rate was 0.049% of initial capacity/per cycle, exerting outstanding cycling stability and high capacity with respect to present work of lithium-sulfur batteries [6,38]. The Coulombic efficiency gradually decreased from 94.4 to 87.6% during the 1000 cycles, indicating the slowly intensified impact of shuttle effect of polysulfides. The Galvanostatic charge–discharge voltage profiles shown in Fig. S2. illustrated a typical feature of two voltage platforms. The lower voltage platform decreased gradually, which is attributed to the irreversible deposition of Li_2S_2 and/or Li_2S in the lithium sulfur cell.

In consideration of the commercial application of Li-sulfur batteries, a high sulfur content of 80% in CNT@S composites was also investigated. With the increase of sulfur content from 50 to 80% according to the TGA, the areal density of sulfur was enhanced from 0.42 to 1.48 mg cm^{-2}. As shown in Fig. S3, a similar relationship between the initial and 10th discharge capacity at a current rate of 0.1 C vs. the sulfur loading amount was observed. The [S] of 1.37 M demonstrated an optimal performance in the concentration of 0.41–5.22 M.

To improve Coulombic efficiency and demonstrate the general phenomena of the effect of sulfur/electrolyte loading, the $LiNO_3$ was introduced into the electrolyte to help the formation of stable solid electrolyte interface films at both the cathode and anode and selective deposition of polysulfide on the cathode [31,39], leading to the increase of Coulombic efficiency. The polysulfides were also introduced to prevent the performance degradation inherent to Li–S batteries by self-healing effect [40]. However, the polysulfides attended to be reduced to lithium sulfides/disulfides, which contributed to the discharge capacity. Herein, the amount of polysulfides should be also considered as the effective sulfur addition and calculated into the sulfur loading concentration.

As shown in Fig. 2a, the discharge capacities of 373, 620, 965, 1086, and 158 mAh g^{-1} (all based on the total mass of sulfur in both cathode and polysulfide-containing electrolyte) were available at the sulfur loading concentration of 0.59, 0.79, 1.12, 1.67, 3.23 mol L^{-1}, respectively. Attributed from the competitive adsorption and reaction of polysulfide and $LiNO_3$ on the Li anode, the Coulombic efficiency was still low, and the corresponding shuttle factor was higher than 0.3. There was still an optimized ratio of sulfur/electrolyte loading to obtain high discharge capacity and low shuttle factor. As shown in the 2nd cycle of galvanostatic charge–discharge profiles (Fig. S4), the two discharge stages were also illustrated with the reduction of sulfur to polysulfide at 2.33 V and the further reduction of polysulfide into lithium sulfide at 2.10 V. Compared with the electrolyte without polysulfide additives, the capacity contribution of reduction of sulfur to polysulfide decreased obviously (Fig. S5), which was attributed to the fact that the Li_2S_x ($x = 4–8$) species were pre-introduced into the electrolyte, building a high concentration gradient of polysulfides and participating into the electrochemical reduction of polysulfide into lithium sulfide. Interestingly, the shuttle factor decreased to 0.03 after the first cycle, indicating the new-formed Li anode/electrolyte interface was covered by stable Li_xNO_y species from the reduction of $LiNO_3$ [39]. An optimized [S] around 1.67 M was determined

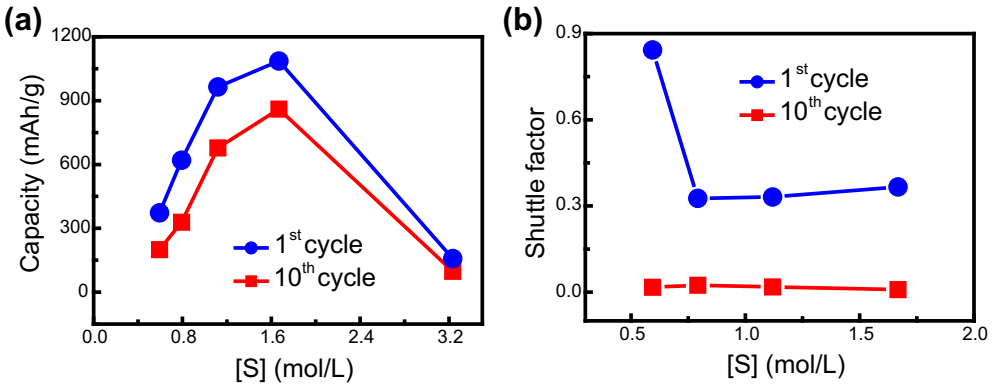

Fig. 2. (a) The relationship between the initial and 10th discharge capacity at a current rate of 0.1 C *vs.* the sulfur loading amount based on Li_2S_x/$LiNO_3$/DME/DOL electrolyte in a Li/S cell. (b) The dependence of shuttle factor on the sulfur loading amount in a Li/S cell.

(Fig. 2) with the highest discharge capacity and lowest decay rate of 2.0%/per cycle during the initial 10 cycles.

The Li storage performance of sulfur cathode highly depended on the loading of sulfur/electrolyte, which can be explained by the following scenarios (Fig. 3). The discharge capacity was attributed from the two-stage multi-electron-transfer reaction. With rising of sulfur loading concentration, the capacity contributed from the high plateau gradually increased and reached a vertex with a sulfur loading concentration of 1.12 mol L^{-1} (Fig. S5). Meanwhile, a minimum polarization of polysulfide reduction was available, and the highest discharging capacity of the CNT@S cathode was illustrated. When the loading amount of sulfur was low, there was a large amount of electrolyte in the cell, which was well distributed in the cathode, membrane, and anode and served as the ion channels. The dissolved polysulfides derived from the reduction of sulfur at the cathode started to diffuse to the Li anode, which was attributed from the large amount of polysulfide anion channels between the cathode and anode. Therefore, the shuttle of polysulfide between cathode and anode consumes the chemical potentials in the cell, but it does not transfer electrons to the external circuit. With the improvement of [S] and the corresponding decrement of electrolyte, the ions conductivity became low, and the ratio of polysulfide diffusion into the anode became smaller, the fully coverage of Li anode by insoluble Li_2S or Li_2S_2 became difficult, and contribution from the following S_n^{2-} react with these fully reduced sulfides to form lower order polysulfides (S_n^{2-}) decreased, as a result, the polysulfide shuttle was retarded. The shuttle of polysulfide can be minimized by increasing the sulfur/electrolyte loading in a cell. Consequently, a Li–S cell with superior capacity performance up to 1000 cycles was available. However, if the sulfur loading higher than 2 mol L^{-1}, the electrolyte can't be uniformly penetrated into the porous cathode and separator, inducing the limited utilization of the active sulfur and poor discharge capacity, although the shuttle of polysulfide was almost fully retarded.

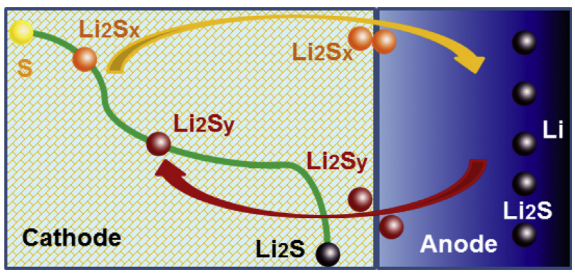

Fig. 3. Schematic illustration of the shuttle of polysulfides in a typical Li/S cells. The shuttle of polysulfides is depended on the ratio of sulfur and electrolytes.

4. Conclusions

The shuttle factor of polysulfide can be mediated from 0.02 to 0.99 by matching the electrolyte/sulfur loading in a Li/S cell. When the loading of sulfur in the electrolyte was 1.12 mol L^{-1}, an initial discharge capacity of 1098 mAh g^{-1} at 0.1 C and a Coulombic efficiency of 97.3% were illustrated on CNT@S cathode in a LiTFSI/DOL/DME electrolyte. For a similar sulfur loading concentration, the 1st and 1000th discharge capacity of 1053 and 535 mAh g^{-1} were delivered and the decay rate is only 0.049%/per cycle during 1000 cycles, which exerts outstanding cycling stability and high capacity with respect to present work of lithium-sulfur batteries. The use of matching the sulfur/electrolyte loading is a facile way to tune the shuttle of polysulfide and the value of [S] varies in different system of Li/S cells. The optimized [S] of coil cells may be much smaller than that of the packing cells and even the practical application, because of there is dead volume in a coil cell and the difference in the amount of liquid holdup of the various electrode materials and membranes. In any case, the principle discussed above is significant both in theory and practical application of Li/S cells, which provides not only new insights to the energy chemistry of Li/S batteries, but also important principles to assemble a Li/S cell with recommended loading for their commercialization application in portable mobile devices and electric vehicles. The distribution inside the cell and consumption process of electrolyte during the cycles should be further explored.

Acknowledgements

This work was supported by National Basic Research Program of China (973 Program, 2011CB932602), China Postdoctoral Science Foundation (2012M520293, 2013T60125), and the National Natural Science Foundation of China (21306103).

Appendix A. Supplementary data

Supplementary data related to this article can be found at http://dx.doi.org/10.1016/j.jpowsour.2013.12.031

References

[1] G. Zhou, L.-C. Yin, D.-W. Wang, L. Li, S. Pei, I.R. Gentle, F. Li, H.-M. Cheng, ACS Nano 7 (2013) 5367–5375.

[2] D.W. Wang, Q.C. Zeng, G.M. Zhou, L.C. Yin, F. Li, H.M. Cheng, I.R. Gentle, G.Q.M. Lu, J. Mater. Chem. A 1 (2013) 9382–9394.
[3] Y.Z. Fu, Y.S. Su, A. Manthiram, ACS Appl. Mater. Interfaces 4 (2012) 6046–6052.
[4] S.S. Zhang, J. Power Sources 231 (2013) 153–162.
[5] Y. Yang, G.Y. Zheng, Y. Cui, Chem. Soc. Rev. 42 (2013) 3018–3032.
[6] A. Manthiram, Y.Z. Fu, Y.S. Su, Acc. Chem. Res. 46 (2013) 1125–1134.
[7] X.L. Ji, L.F. Nazar, J. Mater. Chem. 20 (2010) 9821–9826.
[8] X.L. Ji, K.T. Lee, L.F. Nazar, Nat. Mater. 8 (2009) 500–506.
[9] S. Xin, Y.X. Yin, L.J. Wan, Y.G. Guo, Part. Part. Syst. Char. 30 (2013) 321–325.
[10] D. Li, F. Han, S. Wang, F. Cheng, Q. Sun, W.C. Li, ACS Appl. Mater. Interfaces 5 (2013) 2208–2213.
[11] F.G. Sun, J.T. Wang, H.C. Chen, W.C. Li, W.M. Qiao, D.H. Long, L.C. Ling, ACS Appl. Mater. Interfaces 5 (2013) 5630–5638.
[12] G.M. Zhou, D.W. Wang, F. Li, P.X. Hou, L.C. Yin, C. Liu, G.Q. Lu, I.R. Gentle, H.M. Cheng, Energy Environ. Sci. 5 (2012) 8901–8906.
[13] S. Dorfler, M. Hagen, H. Althues, J. Tubke, S. Kaskel, M.J. Hoffmann, Chem. Commun. 48 (2012) 4097–4099.
[14] X.F. Liu, Q. Zhang, J.Q. Huang, S.M. Zhang, H.J. Peng, F. Wei, J. Energy Chem. 22 (2013) 341–346.
[15] M. Hagen, S. Dorfler, H. Althues, J. Tubke, M.J. Hoffmann, S. Kaskel, K. Pinkwart, J. Power Sources 213 (2012) 239–248.
[16] G.Y. Zheng, Q.F. Zhang, J.J. Cha, Y. Yang, W.Y. Li, Z.W. Seh, Y. Cui, Nano Lett. 13 (2013) 1265–1270.
[17] J.Q. Huang, X.F. Liu, Q. Zhang, C.M. Chen, M.Q. Zhao, S.M. Zhang, W.C. Zhu, W.Z. Qian, F. Wei, Nano Energy 2 (2013) 314–321.
[18] H. Wang, Y. Yang, Y. Liang, J.T. Robinson, Y. Li, A. Jackson, Y. Cui, H. Dai, Nano Lett. 11 (2011) 2644–2647.
[19] L.W. Ji, M.M. Rao, H.M. Zheng, L. Zhang, Y.C. Li, W.H. Duan, J.H. Guo, E.J. Cairns, Y.G. Zhang, J. Am. Chem. Soc. 133 (2011) 18522–18525.
[20] M.Q. Zhao, X.F. Liu, Q. Zhang, G.L. Tian, J.Q. Huang, W.C. Zhu, F. Wei, ACS Nano 6 (2012) 10759–10769.
[21] F. Bottger-Hiller, P. Kempe, G. Cox, A. Panchenko, N. Janssen, A. Petzold, T. Thurn-Albrecht, L. Borchardt, M. Rose, S. Kaskel, C. Georgi, H. Lang, S. Spange, Angew. Chem. Int. Ed. 52 (2013) 6088–6091.
[22] J.L. Wang, J. Yang, J.Y. Xie, N.X. Xu, Adv. Mater. 14 (2002) 963.
[23] L.F. Xiao, Y.L. Cao, J. Xiao, B. Schwenzer, M.H. Engelhard, L.V. Saraf, Z.M. Nie, G.J. Exarhos, J. Liu, Adv. Mater. 24 (2012) 1176–1181.
[24] L. Wang, X.M. He, J.J. Li, M. Chen, J. Gao, C.Y. Jiang, Electrochim. Acta 72 (2012) 114–119.
[25] S.M. Zhang, Q. Zhang, J.Q. Huang, X.F. Liu, W.C. Zhu, M.Q. Zhao, W.Z. Qian, F. Wei, Part. Part. Syst. Char. 30 (2013) 158–165.
[26] X.L. Ji, S. Evers, R. Black, L.F. Nazar, Nat. Commun. 2 (2011) 325.
[27] E.S. Shin, K. Kim, S.H. Oh, W. Il Cho, Chem. Commun. 49 (2013) 2004–2006.
[28] J.T. Lee, Y. Zhao, S. Thieme, H. Kim, M. Oschatz, L. Borchardt, A. Magasinski, W.I. Cho, S. Kaskel, G. Yushin, Adv. Mater. 25 (2013) 4573–4579.
[29] L.M. Suo, Y.S. Hu, H. Li, M. Armand, L.Q. Chen, Nat. Commun. 4 (2013) 1481.
[30] S.S. Zhang, Electrochim. Acta 97 (2013) 226–230.
[31] S.S. Zhang, Electrochim. Acta 70 (2012) 344–348.
[32] S.S. Zhang, Energies 5 (2012) 5190–5197.
[33] Q. Zhang, J.Q. Huang, M.Q. Zhao, W.Z. Qian, F. Wei, ChemSusChem 4 (2011) 864–889.
[34] Q. Zhang, J.Q. Huang, W.Z. Qian, Y.Y. Zhang, F. Wei, Small 9 (2013) 1237–1265.
[35] Q. Zhang, M.Q. Zhao, J.Q. Huang, Y. Liu, Y. Wang, W.Z. Qian, F. Wei, Carbon 47 (2009) 2600–2610.
[36] J.Q. Huang, Q. Zhang, S.M. Zhang, X.F. Liu, W.C. Zhu, W.Z. Qian, F. Wei, Carbon 58 (2013) 99–106.
[37] Y.V. Mikhaylik, J.R. Akridge, J. Electrochem. Soc. 151 (2004) A1969–A1976.
[38] M.K. Song, E.J. Cairns, Y.G. Zhang, Nanoscale 5 (2013) 2186–2204.
[39] D. Aurbach, E. Pollak, R. Elazari, G. Salitra, C.S. Kelley, J. Affinito, J. Electrochem. Soc. 156 (2009) A694–A702.
[40] R. Xu, I. Belharouak, J.C.M. Li, X. Zhang, I. Bloom, J. Bareño, Adv. Energy Mater. 3 (2013) 833–838.